

# A Multi-Layered Image Cache for Scientific Visualization

Eric LaMar

## ABSTRACT

We introduce a multi-layered image cache system that is designed to work with a pool of rendering engines to facilitate an interactive, frameless, asynchronous rendering environment. Our system decouples the rendering from the display of imagery. Therefore, it decouples render frequency and resolution from display frequency and resolution, and allows asynchronous transmission of imagery instead of the compute–send cycle of standard parallel systems. It also allows local, incremental refinement of imagery without requiring all imagery to be re-rendered. Images are placed in fixed position in camera (vs. world) space to eliminate occlusion artifacts. Display quality is improved by increasing the number of images. Interactivity is improved by decreasing the number of images.

**keywords:** image cache, impostors, scientific visualization, multi-resolution techniques, hierarchical techniques, parallel techniques.

## 1. INTRODUCTION

In this paper, we consider the problem of providing a simple and general solution to the problem of scaling the performance of a graphics system with respect to large variations of the input data set and the resources available. Given a basic rendering engine, it is a major task to provide scalability of the engine’s performance with respect to (i) size of the input dataset, (ii) resolution of the output display and (iii) amount of computational resources available (including parallel and distributed processing units, memory, and hardware acceleration). In a complex system, this task may also be replicated several times as several rendering engines are used concurrently (such as slicing, volume rendering, and iso-contouring). Previous parallel rendering techniques are based on a compute–send–display cycle that must be executed strictly within the time elapsed between the display of two frames. That is, while the parallel rendering engines are producing images, the network is not being used. When rendering of the images is complete, all of the render engines synchronize; the slowest engine therefore determines the overall time that is used to produce images. The previously idle network then becomes saturated with traffic as the images are all sent at the same time. The network is being used very inefficiently as it alternates between disuse and over use.

Caching and reusing imagery over several display cycles relaxes the requirement that all images be re-

rendered every frame. Moreover, the images can be sent continuously, thereby spreading the load over time and utilizing the communications resources more efficiently. This generation of images without a strict sense of a frame is called “frameless rendering.”

There is a large body of research on using impostor images generated off-line to approximate large scenes that cannot be rendered interactively. However, existing techniques are unable to meet the demands of scientific visualization in that they expect static scenes, and require significant preprocessing time and user assistance to place impostors. Scientific visualization methods require user-controlled, run-time parameters that can significantly alter the visualization results, *i.e.*, transfer-functions for volume visualization, iso-value for iso-contouring, or temporal movement for time-varying datasets. All of these require adaptive refinement and dynamic updating of the imagery.

**Outline of the approach.** We have developed our Multi-Layered Image Caching (MLIC) system to cache rendered images and to address issues specific to the use of impostors for scientific visualization. The components of our system include a display engine, an image database, and a set of rendering engines. Our system uses a special decomposition of space about the viewpoint: the first is to refine the space into a set of non-occluding (with respect to the viewpoint) polyhedra. These polyhedra are then refined by an individual k-D tree to allow for adaptivity. As the viewpoint moves, so do the polyhedra and k-D trees move.

Each node of the k-D trees has an associated image produced from the data enclosed by that node; the images have specific spatial position and extent.

The images all have the same pixel resolution, so low-resolution regions are covered by fewer images with larger spatial extent, and high-resolution regions are covered by more images with smaller spatial extent.

The images can overlay each other with respect to the viewpoint, so they include both color and opacity information. The images cover the space around the viewpoint, although only those currently visible in the camera’s view frustum are displayed. The images do not move with respect to the viewpoint (or each other), so do not include depth information.

The rendering engines receive requests to generate new images. Upon completion, they send an acknowledgment to the display engine and send images to the image database.

By combining an image database, a display engine that displays only what is available, and the explicit notification of render requests and acknowledgments, the MLIC system accomplishes the decoupling of image display rates from image generation rates. The decoupling of display resolution from rendering resolution is accomplished by images covering different spatial extents. Local refinement of data does not require re-rendering all images. Instead, only those images that intersect the refinement region need to be re-rendered.

As the images are held at fixed positions with respect to the viewpoint, a translation of the viewpoint through the data means that images have also moved from where they were rendered. These images should be re-rendered; however, if the translation is small, they can be used to approximate the correct image. Hence, if the rate at which images can be re-rendered is slow, and the viewpoint is moving slowly, not all images need be re-rendered each display cycle.

The display engine displays images from the image database. It iterates through the set of polyhedra that decompose the space about the viewpoint. For each polyhedra in the view frustum, traverse the associated k-D tree, displaying images that meet the current display requirements. If an image does not meet display requirements (*i.e.*, it was generated when the viewpoint was at a different location or it covers too large a spatial extent), the display engine sends a request to the render engines to generate one or more new images. When these new images are available, the display engine displays them.

**Main Results.** We have implemented a parallel shared memory and distributed MPI versions of our MLIC system, on an SGI Origin3000 and a Linux cluster, respectively. Our intent is to provide interactive rendering of large datasets and linear scaling on the number of rendering engines. Both implementations show linear scaling for some modest-sized ( $512^3$ ) datasets.

We currently use VTK for rendering because it supports a very large array of rendering modalities. However, none of the modalities is very fast, and VTK cannot seem to handle datasets larger than  $512^3$ .

Both implementations use simple FIFO queues for render requests and acknowledgments. When moving through a dataset quickly and displaying it at high resolution (*i.e.*, displaying a large number of images), the rendering engines are not able to re-render images from the current viewpoint quickly enough to produce a consistent view of the data (*i.e.*, all the images are from slightly different locations). This can make it difficult

to navigate through the dataset. Prioritizing re-render requests to provide a consistent view for the very center of the display, while letting the periphery be less consistent, could make navigation easier. Similarly, predicting the viewpoint location would allow generation of images that will be correct.

## 2. RELATED WORK

In this section we discuss related works in the areas of parallel and distributed rendering, image-based rendering techniques, multiresolution data structures, specialized hardware, and other related techniques.

### 2.1. Parallel and Distributed Rendering

Ma *etal.*<sup>1</sup> introduces Binary-Swap composition to reduce the total amount of imagery sent over the network of a parallel machine when performing parallel, distributed rendering. The data are distributed as thin slabs that cover the viewport. Instead of each node transmitting its entire image to one common node to be composited, the images are composited in a binary tree hierarchy. The authors implemented their system on a Connection Machines CM5 and did not discuss issues with other communication topologies.

Parker *etal.*<sup>2</sup> discuss parallel isosurface computation on an Origin2000. They observe that while ray-tracing has a high per-instance cost, it is extremely parallelizable. They use a two-level hierarchy to enable skipping of empty space, and observe near-linear scaling, and a 10 frames-per-second visualization, on the 1GB Visible Woman dataset. Their technique relies on the data to be a regular, Cartesian grid, for efficient traversal and iso-contour tests.

Ahrens *etal.*<sup>3</sup> discuss parallelizing the general datapath of Kitware’s (VTK) Visualization Toolkit, with the goal of visualizing extremely large datasets on large, parallel machines. The current MPI extensions to VTK only parallelize individual filter modules. Their system shows reasonable, but sub-linear, scaling.

Wald *etal.*<sup>4</sup> discuss the parallelization of a highly optimized ray-tracer on a cluster of PCs. Scenes with millions of triangles can be ray-traced at several frames per a second. They show linear speed-up up to 16 nodes, when the display node’s network connection becomes saturated. Scene data is replicated on all nodes, so their system does not scale with respect to data.

### 2.2. Image-Based Rendering Techniques

**Light-Field Techniques.** There are several techniques that can create a novel view of an object of scene from a set of pre-computed, pre-recorded views. Gortler *etal.*<sup>5</sup> and Levoy *etal.*<sup>6</sup> demonstrate the efficacy of “light-field” techniques (so called because they attempt to represent all of the possible light rays in a

scene, a 5D function). Both techniques use simplifying assumptions to reduce the dimensionality of the function and make the problem tractable. Images can either be synthetic or of a real-world object. A new image is generated for a new viewpoint by blending images from near-by viewpoints. Neither technique is able to handle large differences between images.

**Layered Images.** Several software techniques have been designed to decompose a scene into layers, then display the layers from viewpoints close to the original. Mueller *etal.*<sup>7</sup> allow transparent volume visualization, but must keep track of all composited depth values, so the system can place the layers such that no gaps appear when viewing the layers from new viewpoints. Schauffer<sup>8</sup> uses multiple layers to render fully opaque models. Gaps are avoided by overlapping the spatial extents of the layers such that the images overlap by several pixels. Layers are re-rendered just before a gap is predicted to appear. His prediction mechanism only characterizes error with respect to camera translations and not with camera rotations about the model. Shade *etal.*<sup>9</sup> discuss techniques to use layers of images (with color and depth) to approximate complex objects. Images are re-projected on a pixel-by-pixel basis and require a well-defined depth value; this technique is useful only for fully opaque objects.

**Impostors.** A significant amount of work<sup>10-14</sup> has been done on the use of impostors for viewing extremely large architecture walk-throughs, either of individual buildings, or of whole cities or city districts. Significant preprocessing effort (with user assistance) is required to find good locations to place impostors and to segment the model, with respect to the impostor’s location, to near and far sets. Far geometry is rendered and cached with that impostor. At run-time, near geometry is rendered directly and the far geometry is approximated with the cached imagery.

### 2.3. Multi-Resolution Data Structures

**Octrees.** Shekar *etal.*<sup>15</sup> discuss an octree-based iso-surface decimation approach. A seed-cell and surface tracking technique is used to extract the initial surface. The geometry is then progressively decimated and stored at different levels of the octree. They also describe how to patch the surface between different levels of detail without cracks or introducing more triangles.

LaMar *etal.*<sup>16</sup> introduce multiresolution volume visualization techniques. The data volume is decomposed by an octree into a hierarchy of approximations. Original data is stored in leaf nodes, and approximations are stored in interior nodes; the root node contains

the coarsest approximation. To generate an approximation to render, the octree is traversed from root to leaf nodes, adding nodes to the approximation, until error criteria or rendering budgets are met.

**Adaptive Mesh Refinement (AMR).** AMR<sup>17</sup> is a technique used in CFD (computation fluid dynamics) simulations where interesting phenomena vary significantly in spatial extent. Compared to “regular” refinement approaches (*i.e.*, octrees), AMR more closely resembles a “soup of nested grids.” This “soup” is refined around regions of interest and coarsened elsewhere. This refinement/coarsening can occur each time step.

Bethel *etal.*<sup>18</sup> discuss the Visipult system, a distributed volume visualization system for time varying AMR datasets. Imagery is produced at the brick-level and is not independent of the data decomposition.

Weber *etal.* discuss iso-surface extraction<sup>19</sup> AMR grids, with the emphasis of maintaining  $C^0$  continuity across boundaries of bricks of different resolutions. Continuity requires computing a dual grid of the AMR grid, computing a set of “stitching” cells, then extracting geometry from the grid voxels and “stitching” cells.

### 2.4. Specialized Hardware

Numerous specialized hardware solutions have been proposed to parallelize rendering of large datasets or to drive large display walls.

There are several research projects<sup>20-22</sup> that have explored using COTS (common off the shelf) desktop machines with specialized interconnects to improve rendering speeds. The first two use a  $M \times N$  cross-bar switch to connect  $M$  PCs to  $N$  display devices. The latter connects  $N$  machines in a daisy chain. The first allows adaptivity with respect to image size and location, but is only a software simulation. The latter two allow very limited adaptivity with respect to image size and location. All of these can scale if only one of render size ( $M$ ), display size ( $N$ ), or data size is scaled up, but do not scale if all are increased.

The SGI Origin systems, equipped with InfiniteReality<sup>23</sup> rendering engines, provide a general solution to parallel rendering. While they have a extremely fast interconnect fabric, the InfiniteReality engine is much slower than newer cards and only a few can be installed in a single machine. The PixelFlow<sup>24</sup> uses a deeply pipelined compositing network connected to a set of rendering engines. Data is distributed over the rendering engines, which compute a full frame, and ship the frame to the compositing network.

All of the hardware techniques show reasonable speed-ups for small numbers of rendering engines, dis-

plays, and datasets, but extremely expensive and very specialized. These systems have an explicit notion of frames and are not tolerant of delays or stalls in rendering engines. Two recent commercial products, SGI's InfinitePerformance and HP's SV6 use a larger number of rendering nodes, connected by a compositing network. While neither are COTS, both are more commodity- and component-oriented than prior offerings by SGI and HP.

### 2.5. The MLIC Technique

While our technique relies on a set of parallel processes to quickly produces images, it does not require an explicit notion of frames, thus avoiding the communications loading of the compositing phase of traditional parallel rendering techniques. Our technique also uses impostors - cached images. However, it only caches run-time generated imagery - there are (and can be) no preprocessed images. The rendering engines can use any form multiresolution representation or any kind of rendering technique "under the hood" without affecting the design or operation of any other component of the system. The image database is a hierarchical data structure, but we use the term "multi-layered" to differentiate it from multi-resolution rendering or datasets. Our system requires not rely on any special hardware, so it does not have the cost consideration of specialized hardware solutions. However, the faster the network and processors, the better our system will fair. Our system requires no preprocessing of the data, nor generation of any imagery before exploring a dataset. All cached imagery is imagery produced during the exploration of the dataset.

## 3. THE MLIC SYSTEM

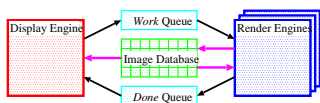


Figure 1. The conceptual MLIC system structure.

Figure 1 shows the conceptual structure of our MLIC system. The display engine (shown in red) displays images from the image database (shown in green). It sends requests for images via the *work* queue (shown in cyan) to the render engines (shown in blue). Upon completing an image, the render engines sends the image to the image database, and sends an acknowledgment via the *done* queue (also shown in cyan). The purple lines show image movement, and the black lines show movement of requests and acknowledgments.

### 3.1. Foundations

Understanding the design of the MLIC requires understanding the method and reason for decomposing the space about the view-point. We draw a distinction between images and k-D nodes, how the image database and the k-D tree decomposition of space are traversed, and the operations required to maintain both.

#### 3.1.1. View Dependent Space Decomposition

One issue with prior techniques is that densely placed images that move with respect to the view-point commonly experience occlusion artifacts. Images that are supposed to be adjacent to each other can appear to move apart, allowing a hole to form where structures that are supposed to be hidden are exposed, or adjacent images move over and occlude each other, as shown in Figure 2. While these problems have been addressed in a very basic way for opaque structures, there are no prior techniques to handle transparent structures.

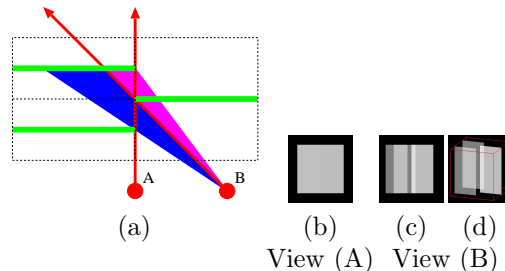
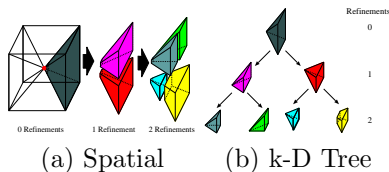


Figure 2. Occlusion artifacts occur when images generated to be correct from view-point *A* are viewed from view-point *B*. In (a), view-points are red, images are green, the hole is blue, and the occlusion is magenta. (b)-(d) shows (a) from the view-point; the two left images have opacities of 50% (which composite to opacity of 75%), and the right image has an opacity of 75%.

Our solution is to decompose the space around the view-point into a set of convex, non-occluding (with respect to the view-point) polyhedra, which are then refined by a k-D tree to allow for adaptivity. The k-D tree based refinement of the polyhedra is constrained to avoid these occlusion artifacts. Images are placed at the nodes of the k-D tree and move with the view-point.

The implementations discussed in this paper uses a cube, centered about the view-point, decomposed with six pyramids, where the tops meet at the view-point and the bases form the six faces of the cube. Other configurations are possible. Figure 3 shows a cube, centered around the view-point (shown as a red disk) decomposed into six polyhedra. One polyhedra (shown in purple) is then refined twice by a k-D tree. The tree on the right shows the parent-child relationships between the nodes.



**Figure 3.** Example of the decomposition of a cube about the view-point (the red circle) into six polyhedra (pyramids). (a) shows the spatial decomposition, while (b) shows the k-D tree representation of the decomposition. The gray pyramid is refined twice.

The images are placed at fixed positions with respect to the view-point, so must be re-rendered when the view-point translates; they don't need to be re-rendered if the view-point's orientation or view-frustum change.

Figure 4 shows a 2D and 3D example of a Multi-Level Image Cache implemented using a square/cube basis. For figure 4(a), the red disk at the center is the view-point. The red lines show the view frustum. Black lines show the base pyramid decomposing of the space; blue lines show the k-D tree refinement of each pyramid; and green lines show individual images. The images are shown slightly smaller than their physical extent (delimited by blue and black lines) to emphasize that they are independent entities. Note that the different pyramids have different levels of refinement. Figure 4(b) shows the pyramids in different colors, and scaled down by 10% to show the individual nodes. All pyramids have been refined twice.

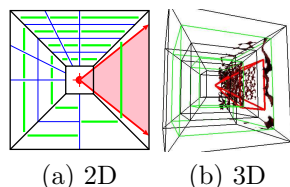


**Figure 4.** Example of a MLIC implemented (a) on a square in 2D and (b) on a cube in 3D. In both, the view-point and view-frustum is illustrated with red pyramid. Figure (a) shows that the different polyhedra can have different degrees of refinement by a k-D tree. Figure (b) shows all six polyhedra with one front/back refinement.

The distance to the outer face of a pyramid corresponds to the far-clipping plane of a viewing-frustum. Increasing and decreasing the distance to the far-clipping plane increases and decreases the spatial extent covered by the cache.

The k-D tree refinement planes are either parallel to the cube face or pass through the origin of the cube, so there are no occlusion artifacts (compared to Figure 2); *i.e.*, images about the boundaries of a k-D node and their end-points do not move with respect to the view-

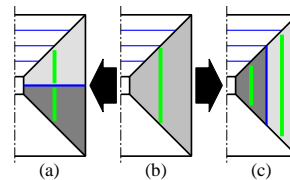


**Figure 5.** A k-D tree node can be refined along two orientations in 2D (three in 3D). (b) is the parent; (a) shows a left/right or top/bottom split, while (c) shows a front/back split.

point. This is shown in Figure 5. Figure 5(b) shows the parent image to be refined; Figure 5(a) shows the refinement of the parent image parent image into left and right images. This can also be see in Figure 3(a) with the gray to red/purple split or the red to gray/green split. Figure 5(c) shows the refinement of the into front and back images (with respect to the view-point), also shown in Figure 3(a) with the red to cyan/yellow split.

**Images vs. k-D Nodes.** One distinction that we need to make between images and k-D nodes. While there is a one-to-one correspondence of images in the image database to nodes in the k-D tree decomposition of the polyhedra about the view-point, they are conceptual different entities.

The k-D tree decomposes space into a set of sub-regions; in our system, all of these regions are hexahedral trapezoids. The image associated with a node of the k-D trees contains the rendered view of the data enclosed by that k-D node. If the view-point translates, the k-D node is not changed, but the image may change. Also, if data viewing parameters are changed, *e.g.* the transfer function or iso-contour value, the image will change but the k-D node will remain unchanged.

Secondly, the display engine may only display a small portion of the images in the image database. While there might be a higher-resolution decomposition of some region, the display engine, for reasons of rendering budget, or some other, may choose not to show all of the images in the image database. At the same time, there is a difference between the refinement that the display engine performs to display some portion of the image database, and the refinement of the images in the image database itself: the former modifies what is displayed from, and the latter modifies what is contained in, the image database.

**Image Reuse.** Figure 6 shows where images would be reused after rotating the view-frustum. In Figure 6(a) the first frame, a set of images in rendered. The blue and green images are rendered for the first frame. In the second frame (Figure (b)), as the view-frustum

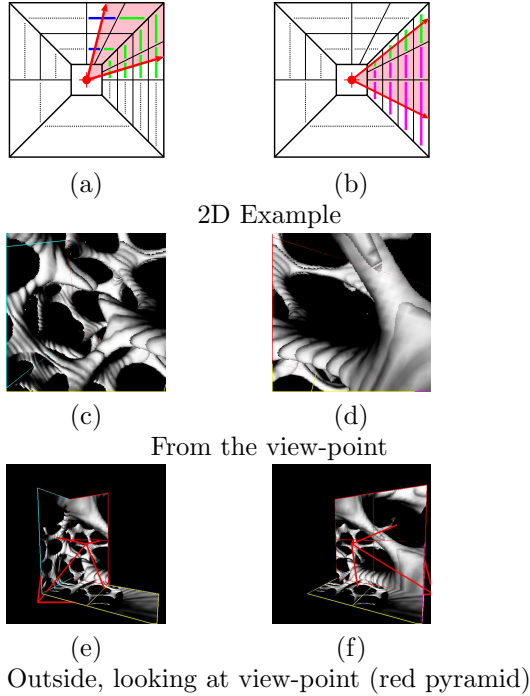


**Figure 6.** Reusing images as the view-frustum turns to the right.

turns right, an additional set of images is now visible. Those shown in green are rendered in both frames. Images shown in blue are not visible in the second frame, and may be deleted (if running out of cache space). The purple images in the second frame are now visible; they will be placed in a *work* queue to be rendered if the images are invalid. The middle row shows a rendering of a iso-surface rendering of a Trabecular bone dataset; the initial view-point position is shown in the left image (c) and the view-frustum has turned to the right in the right image (d). The bottom row shows a side view of the MLIC refinement, with the view-point and view-frustum pyramid shown in red. Image boundary color corresponds to the faces of the cube. Notice that the images outlined in cyan no longer appear in the right image, and new images appear on the right side of the image.

All images have the same resolution. A k-D tree node is refined by replacing it with a left/right, top/bottom, or front/back child, where each child node’s images contains a copy of the corresponding region of the parent node’s image. The new images are marked for future re-rendering. Images are coarsened by removing the child nodes and replacing the parent’s imagery by a filtered version of the child node’s images.

Rotating the view-frustum direction does not invalidate any of the images, but newly exposed images may require rendering, and possibly refinement.

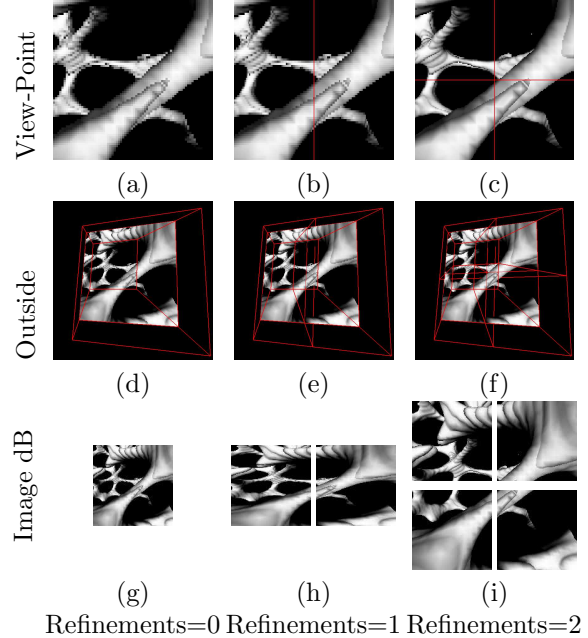


**Figure 7.** Three levels of refinement, showing left/right and top/bottom splits of the image database and k-D nodes.

Figure 7 shows examples of refining the image database and k-D tree. Figure 7 shows three levels of refinement of the image database and k-D tree, demonstration left/right and top/bottom splits. The first column (Figures 7(a,d,g)) shows a single image with no refinement. The second column (Figures 7(b,e,h)) shows a left/right split, and the third column (Figures 7(c,g,i)) shows a further top/bottom split. The first row (images 7(a)-(c)) show the scene from the view-point. The second row (images 7(d)-(f)) show the scene from outside the view-point; the red lines show the borders of the k-D nodes and the images. The third row (images 7(g)-(i)) show the individual images in the image database. Notice that the sub-images of image 7(h) are stretched; this is because they cover less space left-to-right than top-to-bottom.

### 3.1.2. Displaying the Image Database.

The space about the view-point is decomposed by polyhedra, then refined by k-D trees. Displaying the image database involves visited all the polyhedra, and traversing the accompanying k-D trees, in an top-down manner (with respect to the k-D trees) and back-to-front (with respect to the view-point). At each k-D tree node, the image is examined; If the image is current, and it is too coarse, and it has children, then its children are visited. If the image is invalid, then the refinement stops. The image is displayed, and it is tagged to be *rendered*. If the imagery is invalid, and has children, and the children have current imagery, the image is drawn, and the

image is tagged to be *merged*. If the imagery is current, and it is too coarse, it is drawn and it is tagged to be *refined*. If the imagery is current, and it is not too coarse, it is simply displayed.

As we noted earlier, the set of images displayed is potentially a much smaller set than exists in the image database. For example, if user is exploring a dataset and examining many small features without moving the view-point, once an image is rendered and cached, it does not need to be re-rendered. Thus, it is possible to display significantly more detail. However, if the user moves quickly to another, distant view-point, all of the images will become invalid, and it is better to use a smaller number of images, updated more frequently, to provide the user with proper feedback on their movement through the dataset.

### 3.1.3. Image Database Operations.

Three kinds of operations can be applied to images in the image database and nodes in the k-D tree: *refine*, *render*, and *merge*. The image-level operations are to create new images, either by re-rendering the data, or by reusing some previously computed images. The k-D tree level operations are to add or prune nodes from the tree.

The *refine* operation refines a region: it adds child nodes to the k-D tree node which represents that region, allocates images the image database, and computes images for the child nodes by using just the image of the parent node. Figure 3 shows this for the k-D tree: the initial gray pyramid is refined into red and purple nodes. A image can be split (with respect to the view-point) into a left/right pair (Figure 3, red into cyan and yellow nodes), top/below pair (Figure 3, the gray into red and purple nodes), or front/back pair (Figure 3, purple node into light gray and green nodes). Since all images have the same number of pixels, when a left/right or top/bottom pair is refined, the effect is to double to number of pixels in the direction of the split.

The *merge* operation coarsens a region by collapsing a left/right, top/bottom, or front/back pair into their parent node, and to create a lower-resolution image for their parent node. This is used when the view-point has not changed, but the region is less important (*e.g.*, the user has turned the view frustum away). The left/right and top/bottom pairs are produced by low-pass filtering or sub-sampling, depending on which filtering mode used in the original rendering. Merging a front/back pair requires compositing the front and back pairs together.

The *render* operation generates an image from the data contained within the spatial extent of a k-D node.

The render engine is given a dataset at startup, and receives requests to render specific nodes. At the end of rendering, the image is sent to the image database.

## 4. SYSTEM IMPLEMENTATION

We have implemented two versions of our MLIC system. The first is designed to run on a SMP (Symmetric Multi-processor) machine using shared memory for all communication and the image database. The second version is designed to run on a large distributed-memory parallel machine using MPI (Message Passing Interface) for communication.

There are several engines in these two systems, most of which are used in both versions. The fundamental difference between the distributed, message passing version and the shared memory version, is the “dispatch engine”, a module for interfacing with MPI.

### 4.1. Shared Memory

Shared memory is implemented through the Unix *mmap* function call. On 32-bit machines, the maximum size of a shared memory segment available through this mechanism is 2GB. We have not found this limitation to be a problem.

### 4.2. Image Database

```
enum { TileSize = 128 };
struct Pixel { unsigned char r, g, b, a; };
typedef Pixel PxImg[TileSize][TileSize];
class KdNode
{
public:
    BOOL iscopy; // TRUE when refine or merge
    BOOL inqueue; // TRUE when in done/work queues
    int nodeid; // Identity of this node
    int parentid; // Identity of this node's parent
    int leftid; // Identity of this node's left child
    int rightid; // Identity of this node's right child
    int kd_dir; // The X/Y/Z direction of the split
    int depth; // Depth of this node in the tree
    float pos[3]; // View-point where image was rendered
    PxImg image; // The Image
};
KdNode ImageDb[];
```

**Figure 8.** The Image Database is a large array of *KdNode* structures.

The *image database* is shown in figure 8, and is stored in the shared memory segment. The first *N* positions of the database are the root nodes of the *N* polyhedra that decompose the space about the view-point. Since the current implementation uses a cube, the first six position are the root nodes for the six faces of the cube.

The *inqueue* flag is set to true when a image is first added to the *work* queue, and set to false when it is removed from the *done* queue. This flag used is to prevent a image from being added more than once to the queue.

The *iscopy* flag is set to true if the image was generated through a *refine* or *merge* operation, and false if the image was generated by a *render* operation. If the display engine encounters an image with the *iscopy* flag set to true, the image is displayed, but the render engine adds the image to the *work* queue, requesting a *render* operation on the image.

The *nodeid*, *parentid*, *leftid*, and *rightid* fields are the identifiers (array subscripts) of the current node, its parent node, and its child nodes. The *parentid* field is zero for a root node, and *leftid* and *rightid* fields are both zero for leaf nodes.

The *pos* field records the location of the view-point when the image was rendered. This field is currently used to test if the image is *current*, i.e.,  $pos == \text{current-view-point}$ , or *old*, i.e.,  $pos != \text{current-view-point}$ .

### 4.3. Work and Done Queues

The *work* and *done* queues are implemented as fixed-sized circular queues, and are stored in the shared memory segment. Images that are tagged for one of the maintenance operations are placed (rather, a pointer to the image) in the *work* queue. When the operation is complete, the image(s) are placed in to *done* queue.

### 4.4. Engines

There are three basic engines in the MLIC system: *display*, *render*, and *dispatch*. The first two are found in both implementations, while the latter is only found in the distributed, MPI version.

The *display* engine displays images, and maintains all fields, except for *image*, in the image database. Image operations are requested by the display engine by placing the requests into the *work* queue (and setting the image's *inqueue* flag). When the acknowledgments are received, i.e., read from the *done* queue, the display engine updates the *iscopy* and *inqueue* fields.

The *render* engine performs the image operations and does not modify (in the SMP version) any other fields in the image database. It reads requests from the *work* queue, performs the operation, writes the image(s) to the image database, and send an acknowledgment via then *done* queue.

The *dispatch* engine communicates via the shared memory queues with the display engine and via MPI messages with the render engines. It maintains a queue of currently available render engines. It reads requests from the *work* queue, selects and removes the first entry in the available render engines queue, and sends the render request to that engine. When the acknowledgment comes back, it writes the acknowledgment to the *done* queue, and the image(s) to the image database, and add the render engine back to the available render engines queue.

## 4.5. Shared Memory Implementation

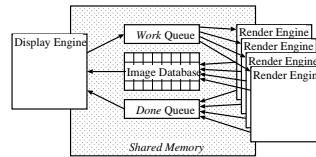


Figure 9. Shared memory architecture.

The shared memory version of MLIC uses a large, shared memory segment that include the image database and the *work* and *done* queues. The display engine and render engines all attach directly to this shared memory segment; see figure 9.

## 4.6. MPI Implementation

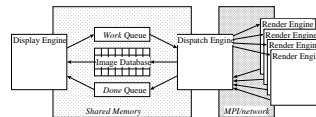


Figure 10. MPI architecture.

The MPI version of MLIC also uses a large, shared memory segment for the image database and *work* and *done* queues. However, there is a third, “dispatch” engine, that moves the requests and acknowledgments from the *work* and *done* queues and the MPI message queues; see figure 10. The display engine is the same code for the shared memory and MPI versions of MLIC.

## 5. MLIC SYSTEM PERFORMANCE

We have tested the shared memory and MPI versions of our MLIC on two different kinds of machines.

### 5.1. Test Platforms

Our first platform is a SGI Origin3000, with 48 250MHz R10K processors and 40GB of memory. The image database and communications mechanisms reside in a large shared memory segment (implemented via *mmap*), with direct access by the viewer and renderer processes. We use software-based ray-casting iso-surfacing and volume visualization engines on this platform, as there are too few graphics pipes to perform a realistic scalability study.

Our second system is a cluster of 64 Linux boxes, connected by a two-level Quadrics network. Each box has two 2.5GHz Pentium Xeon processors, 2GB of memory, a nVidia GeForce ti4600 graphics card, and a Quadrics NIC. The bidirectional bandwidth claimed by the manufacturer is 340MB/sec.

## 5.2. Dataset

We use a Trabecular bone dataset because it is fairly “open,” in that it uniformly covers the full extent of the volume. Thus, we can visually confirm that (1) the decomposition of data space is correct, and (2) the current status of individual images. The original  $540^3$  voxel dataset is  $1\text{ cm}^3$ . We use  $256^3$  and  $512^3$  versions of this larger volume.

## 5.3. Scalability Study.

We study the absolute performance and speed-up characters of the MLIC system on the Origin3000 and Linux cluster, and we show the effect of image size vs. the number of images displayed on display performance. We measure the sustained communications bandwidth of the Linux cluster. We show brief results for the Origin3000 and compare some of these results against the Linux cluster. We show the effect of image size and the number of processors on image rendering performance on the Linux cluster.

### 5.3.1. Display Rates

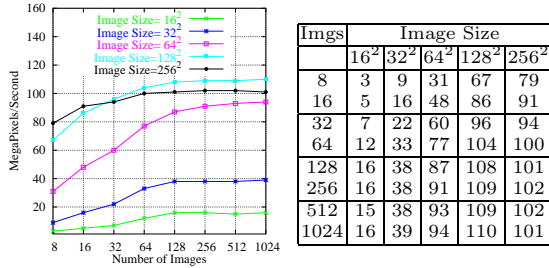


**Figure 11. Display Rates** as a function of total number images displayed and image size. The window size is  $500^2$  pixels. The limiting factor is fill-rate, at about 110 megapixels per a second.

Figure 11 compares the rates for rendering 8 to 1024 images for images of size  $16^2$  to  $256^2$  pixels on a window of  $500^2$  pixels. The images are downloaded as textures, then mapped to a polygon for rendering. Nearest-neighbor filter was used, and mip-mapping was turned off. The “Frame Rate” column reports the number of complete frames rendered per a second. The “Fill Rate” column reports the pixel fill rate in mega-pixels per a second, which is the number of images per a second times the number of pixels per an image. The pixel-fill rates is the best measure of the render capability of the display engine. The numbers reported here, however, reflect both download *and* fill rates because we want measure the worst-case performance. The fill rate tops out at about 110 mega-pixels per a second. The optimum size tile seems to be  $128^2$  pixels, and not  $256^2$ . The decrease at  $256^2$  has to do with the ratio of pixel to texel size and cache-hit rates.

### 5.3.2. Total Communications Bandwidth on the Linux Cluster.

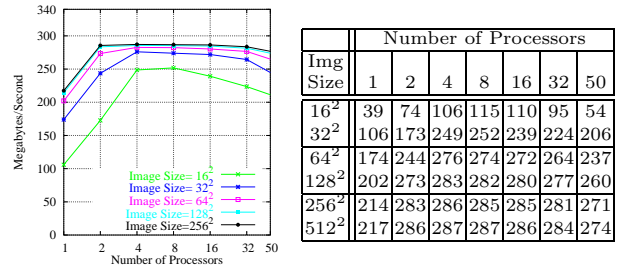


**Figure 12. Total Communications Bandwidth on the Linux Cluster** as a function of image size and number of processors. The numbers shown are Megabytes per second.

This test measures the total effective bandwidth of the Linux cluster for different image sizes and numbers of processors, given the communications behavior of the MLIC system. The observed peak rate of 285MB/second, shown in figure 12, and is very close to the manufacturer’s claimed peak rate of 340MB/second.

The test has the display engine request the rendering of 10,000 images. The rendering engines receive the requests, and immediately send back an empty image. On average, each rendering engine will receive  $10,000/N$  requests, where  $N$  is the number of processors. Each image contains 16 bytes of header and a RGBA image, for a total size of  $(imagesize)^2 \times 4 + 16$  bytes. The Megabytes per second was computed by dividing the total number of bytes sent (total size  $\times 10,000$ ), by the elapsed time from the first request sent by the display engine to the last image received by the display engine. This factors in all of the overhead of MPI, and the sending of the request messages. We do not, however, count the number of bytes in the render request structures because the number of images per second that could be sent *back* to the image database is the only figure of interest.

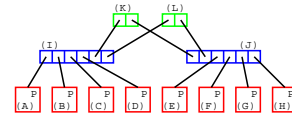


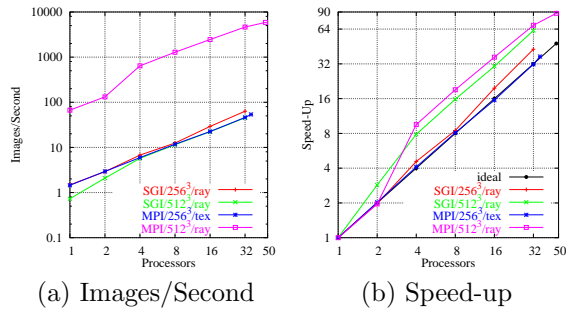
**Figure 13.** A possible Quadrics network configuration, with eight processors and two levels of switches.

The total capacity decreases from 32 to 50 processors due to congestion and contention of the high-level switches. The cluster uses a two-level Quadrics switch network, with eight switches at the highest-level, con-

nected to eight low-level switches (with 8 links to processors and 8 links to high-level switches), for a total of 64 nodes.

Figure 13 shows a simplified network with eight processors (A-H, in red), two low-level switches (I & J, in blue) and two high-level switches (K & L, in green). Links are shown as black lines. The low-level switches have six ports, four to processors, and two to high-level switches. Any packet send between nodes on different low-level switches must pass through the high-level switches. For example, if (A) sends a packet to node (E), it must pass through both low-level switches (I & J) and one of the two high-level switches (K or L). However, if node (A) sends a packet to node (B), the packet must only pass through the (low-level) switch (I). Congestion/contention occurs when the number of nodes attempting transfers across the high-level switches is greater than the number of high-level switches. In our example, this would occur if (E), (F), and (G) all send images to (A) at the same time: one of (E), (F), or (G) would have to wait. Also, if (A) is the display node, then all other nodes are sending data to it and could saturate (A)'s connection.

### 5.3.3. Comparing the Origin3000 vs. the Linux Cluster.



Procs	(A)		(B)		(C)		(D)	
	SGI/256 <sup>3</sup> /ry	SGI/512 <sup>3</sup> /ry	SGI/256 <sup>3</sup> /ry	SGI/512 <sup>3</sup> /ry	MPI/256 <sup>3</sup> /tx	MPI/512 <sup>3</sup> /ry	MPI/256 <sup>3</sup> /tx	MPI/512 <sup>3</sup> /ry
1	1.48	1.00	0.73	1.00	1.45	1.00	67	1.00
2	2.91	1.97	2.09	2.86	2.93	2.02	132	1.96
4	6.76	4.57	5.74	7.86	5.95	4.10	641	9.54
8	12.5	8.47	11.5	15.8	11.8	8.11	1286	19.2
16	29.2	19.7	22.3	30.5	22.5	15.5	2456	36.6
32	63.3	42.8	45.4	62.2	46.0	31.7	4637	69.1
36					53.7	37.1		
50							5885	87.6

(c)

Figure 14. Comparing the Origin3000 vs. the Linux cluster showing images generated per a second and speed-ups using two Trabecular bone datasets. Image Size is 128<sup>2</sup>.

This study compares the absolute render rates and speed-ups on the Origin3000 and Linux cluster. We

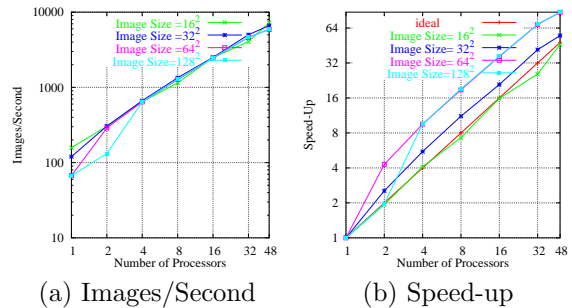
conducted only basic scalability studies on the Origin3000.

Figure 14, columns (A) and (B), shows results using software, iso-surface, ray-casting on the Origin3000, for the 256<sup>3</sup> and 512<sup>3</sup> Trabecular bone datasets, respectively. Figure 14, column (C), shows results of hardware texture volume visualization using the 256<sup>3</sup> dataset, while column (D) shows the results of software, iso-surface ray-casting using the 512<sup>3</sup> dataset, on the Linux cluster. The image size for all of these runs is 128<sup>2</sup> pixels.

Both runs with dataset size of 256<sup>3</sup> exhibit linear scalability, while both with dataset size of 512<sup>3</sup> exhibit super-linear up to four processors, and linear thereafter. We are not sure why the super-linear behavior occurs. Since each processor in both implementations have their own, local copies of the dataset, there should be no super-linear scaling due a distributed dataset fitting into memory caches.

Notice that the two MPI studies use more than 32 processors, but different in the number. This variation is due to the stability and availability of the Linux cluster.

### 5.3.4. Scalability as a function of Image Size vs. Number of Processors.



(a) Images/Second (b) Speed-up

Procs	Image Size							
	16 <sup>2</sup>		32 <sup>2</sup>		64 <sup>2</sup>		128 <sup>2</sup>	
	Img/s	S-U	Img/s	S-U	Img/s	S-U	Img/s	S-U
1	158	1.00	120	1.00	67	1.00	67	1.00
2	304	1.93	306	2.54	289	4.29	132	1.96
4	644	4.09	665	5.53	641	9.51	641	9.54
8	1148	7.28	1341	11.2	1268	18.8	1286	19.2
16	2499	15.9	2508	20.9	2450	36.3	2456	36.6
32	4049	25.7	5010	41.7	4625	68.5	4637	69.1
48	7272	46.1	6619	55.0	5895	87.4	5885	87.6

(c)

Figure 15. Scalability as a function of Image Size vs. Number of Processors collected over the last minute of a four-minute run. (a) shows the rate at which images are processed per a second. (b) shows the speed-up. (c) shows the raw numbers.

This test examines the sustained rate of image generation and transmission on the distributed version of the MLIC implementation, see figure 15. The numbers re-

ported are the sustained rates over the last minute of a four-minute run. The reason that we only measure the last minute is to let the system settle into normal operation. The system takes a minute or two to refine the images to a point where we can reasonably measure of a one-processor run versus a fifty-processor run. Under normal operations, a user would not immediately ask for extremely high-resolution imagery, but only ask for a few images, which can be rendered very quickly. Several of the runs are super-linear up to 4 or 8 processors (rendering engines), and are linear there after. We do not have a good explanation for this apparent super-linear speed-up; however, it seems to be a consistent trend here and in experiments discussed above.

Notice that the capacity of the system does not scale with respect to the image size. This shows that the overhead of the other operations (image read-back, communication, etc.) are large, and are the dominate cost for small image sizes.

Also notice that the speed-up from 32 to 50 processors, while linear, has a smaller slope than the speed-up from 4 to 32 processors. This can be explained by observing that there is a general reduction in bandwidth, starting at 32 processors, as discussed in section 5.3.2.

### 5.3.5. Data Scalability

Our second test (see section 5.3.3) shows that there is basic scalability on the size of the data. However, both datasets are too small, in general, and our tests not comprehensive to make any strong statements about the scalability with respect to dataset size. These two datasets are simply ordered by X, Y, then Z, so extremely large datasets will start to show sub-linear performance due to poor memory locality.

### 5.4. Rendering Requirements vs. Capacity

How many processors and what network bandwidth is necessary? Rather than just discuss the performance of the system from the back-end forward, what are the requirements at the front-end and does the back-end meet them?

If we assume a window of  $1024^2$  pixels, driven by a display engine, how many images it is reasonable to display? If we use a image size of  $128^2$  pixels, the window could be tiled by a  $8 \times 8$  array of images. If, however, we wish to avoid aliasing artifacts, we should use a  $4 \times 4$  array of images, where each pixel in an image projects to (at least) a  $2 \times 2$  array on pixels on the window. This means that the largest dataset that should be displayed on a  $1024^2$  window is  $512^3$ . Notice that we do not say  $512^2 \times X$ , where  $X$  is very large. If a dataset can be viewed from any arbitrary direction, then the largest dimension of the dataset must be 512 or less to satisfy the sampling requirements. This is also not to

say that a larger dataset cannot be handled – only that the *currently displayed* region of the dataset cannot be over  $512^3$  voxels.

If we assume that an image is generated from a cubic subregion of the dataset, then a  $512^3$  dataset is covered by a  $4^3 = 64$  array of images.

If we want each image to be refreshed 30 times a second, then the system must be able to process  $30 \times 64 = 1920$  images per a second. From section 5.3.4, this can be met by only 16 processors.

If we allow aliasing artifacts, we then use  $8^3 = 512$  images, or  $512 \times 30 = 15360$  images per a second. This cannot be met by any configuration, but if we reduce the frame rate to 10 fps, or 5120 images a second, this can just be met.

### 5.5. Bottlenecks

There are two points of limited bandwidth. With a network bandwidth capacity of 285MB/second, the maximum number of pixels received a second at the display engine is 72.12 megapixels/second. The rendering speed tops out a 110 megapixels/second, which is significantly more than the network's 71 Mpx/second ( $= 285MB/s/RGBA$ ). This is a simplistic distillation of the system bottlenecks, but it is clear that there are aspects of the system performance that we do not fully understand.

### 5.6. Observations and Synthesis

The core set of tests show that the system is scalable. However, it is clear that there is a limit to the scalability due to the configuration and capacity of the Quadrics network on our Linux cluster.

For the distributed, MPI, implementation, the primary limitation is the bandwidth to the image database from the rendering engines. The image database is stored in the same machine as the display engine, so all image traffic arrives over a single network connection. There are many possible solutions; the two at the top of our list are compressing the image stream, and using a distributed image cache. While compression is not scalable in the strict sense of the word, it should reduce the traffic. However, will the extra time spent compressing the image be worth it? Our second solution is to use a distributed image cache. That is, use multiple *meta-display* engines, each with its own image database. Render engines send images to one (possibly, more) of these meta-display engines. These meta-display engines when send a partially composited result to the final render engine.

## 6. CONCLUSIONS AND FUTURE DIRECTIONS.

**Conclusions.** We have introduced our Multi-Level Image Caching system as an approach for scaling generic rendering on a parallel, distributed computing system. The MLIC system maintains a set of images for interactive display while a set of parallel engines render new images. Our system has successfully decoupled rendering rates from display rates, allowing for fairly slow image generation, while providing interactive display of imagery. The system experiences linear scaling on an Origin3000 SMP using 32 processors and on a Linux-cluster using 50 nodes.

**Future Directions.** We plan to (1) incorporate multi-resolution render of multi-resolution data sources into the rendering engine. (2) Implement a priority-based scheduler that incorporates error- and view-driven criteria. (3) Add temporal prediction and approximation for time-varying data ( see Nuber *etal.*<sup>25</sup>). And (4), to explore the use of compression and a distributed image cache to ease the communication requirements.

## REFERENCES

1. K. Ma, J. Painter, C. Hansen, and M. Krogh, "Parallel volume rendering using binary-swap compositing," *IEEE CGA* **14**(4), pp. 59–68, 1994.
2. S. Parker, M. Parker, Y. Livnat, P. Sloan, C. Hansen, and P. Shirley, "Interactive ray tracing for volume visualization," *IEEE TVCG* **5**(3), pp. 238–250, 1999.
3. J. Ahrens, C. Law, W. Schroeder, K. Martin, and M. Papka, "A parallel approach for efficiently visualizing extremely large, Time-Varying Datasets," tech. rep., LANL, 2000.
4. I. Wald, C. Benthin, P. Slusallek, T. Kollig, and A. Keller, "Interactive Global Illumination using Fast Ray Tracing," in *Rendering Techniques*, pp. 15–24, June 2002.
5. S. Gortler, R. Grzeszczuk, R. Szeliski, and M. Cohen, "The Lumigraph," in *Siggraph*, pp. 43–54, Aug. 1996.
6. M. Levoy and P. Hanrahan, "Light Field Rendering," in *Siggraph*, pp. 31–42, Aug. 1996.
7. K. Mueller, N. Shareef, J. Huang, and R. Crawfis, "IBR-Assisted Volume Rendering," in *Hot Topics, IEEE Visualization*, pp. 1–4, Oct. 1999.
8. G. Schaufler, "Per-Object Image Warping with Layered Impostors," in *Rendering Techniques*, pp. 145–156, 1998.
9. J. Shade, S. Gortler, L. He, and R. Szeliski, "Layered depth images," in *Siggraph*, pp. 231–242, July 1998.
10. M. Carrozzino, F. Tecchia, C. Falcioni, and M. Bergamasco, "Image caching algorithms and strategies for real time rendering of complex virtual environments," in *Afrigraph*, pp. 65–74, Nov. 2001.
11. B. Chen, J. Swan, II., E. Kuo, and A. Kaufman, "LOD-Sprite Technique for Accelerated Terrain Rendering," in *Visualization*, pp. 291–298, Oct. 1999.
12. G. Schaufler and W. Stürzlinger, "A three-dimensional image cache for virtual reality," in *Eurographics*, 1996.
13. J. Shade, D. Lischinski, D. Salesin, T. DeRose, and J. Snyder, "Hierarchical Image Caching for Accelerated Walkthroughs of Complex Environments," in *Siggraph*, pp. 75–82, Aug. 1996.
14. X. Decoret, F. Sillion, G. Schaufler, and J. Dorsey, "Multi-layered impostors for accelerated rendering," *Computer Graphics Forum* **18**, pp. 61–73, Sept. 1999.
15. R. Shekhar, E. Fayyad, R. Yagel, and J. Cornhill, "Octree-Based Decimation of Marching Cubes Surfaces," in *IEEE Visualization*, pp. 335–344, Oct. 1996.
16. E. LaMar, K. Joy, and B. Hamann, "Multi-Resolution Techniques for Interactive Hardware Texturing-based Volume Visualization," in *IEEE Visualization*, pp. 355–361, 25–29 Oct. 1999.
17. G. Bryan, "Fluids in the Universe: Adaptive Mesh Refinement in Cosmology," *Computing in Science and Engineering* **1**, pp. 46–53, Mar./Apr. 1999.
18. W. Bethel, J. Shalf, S. Lau, D. Gunter, J. Lee, B. Tierney, V. Beckner, J. Brandt, D. Evensky, H. Chen, G. Pavel, J. Olsen, and B. Bodtker, "Visapult - Using High-speed WANs and Network Data Caches to Enable Remote and Distributed Visualization," in *Super Computing*, pp. 118–119, Nov. 2000.
19. G. Weber, O. Kreylos, T. Ligocki, J. Shalf, H. Hagen, B. Hamann, and K. Joy, "Extraction of Crack-free Isosurfaces from Adaptive Mesh Refinement Data," in *VisSym*, pp. 25–34, May 2000.
20. W. Blanke, C. Bajaj, D. Fussell, and X. Zhang, "The Metabuffer: A Scalable Multiresolution Multidisplay 3D Graphics System Using Commodity Rendering Engines," Tech. Rep. TR2000-16, U. Texas, Austin, 2000.
21. G. Stoll, M. Eldridge, D. Patterson, A. Webb, S. Berman, R. Levy, C. Caywood, M. Taveira, S. Hunt, and P. Hanrahan, "Lightning-2: A High-Performance Display Subsystem for PC Clusters," in *Siggraph*, pp. 141–148, Aug. 2001.
22. S. Lombeyda, L. Moll, M. Shand, D. Breen, and A. Heirich, "Scalable Interactive Volume Rendering Using Off-the-Shelf Components," in *IEEE PVG*, pp. 115–121, 158, Oct. 2001.
23. J. Montrym, D. Baum, D. Dignam, and C. Migdal, "InfiniteReality: A Real-Time Graphics System," in *Siggraph*, pp. 293–302, Aug. 1997.
24. J. Eyles, S. Molnar, J. Poulton, T. Greer, A. Lastra, N. England, and L. Westover, "PixelFlow: The Realization," in *Graphics Hardware*, pp. 57–68, 1997.
25. C. Nuber, E. LaMar, and K. Joy, "Approximating time-varying multiresolution data using error-based temporal-spatial reuse," in *Geom. Modeling for Sci. Vis.*, 2003.